Lab on a Chip

Cite this: *Lab Chip*, 2012, **12**, 2046–2052

www.rsc.org/loc

PAPER

Impedance measurement technique for high-sensitivity cell detection in microstructures with non-uniform conductivity distribution†

Andrea Faenza,*[a] Massimo Bocchi,[ab] Nicola Pecorari,[a] Eleonora Franchi[a] and Roberto Guerrieri[a]

Received 13th February 2012, Accepted 22nd March 2012
DOI: 10.1039/c2lc40158d

Particle detection in microstructures is a key procedure required by modern lab-on-a-chip devices. Unfortunately, state of the art approaches to impedance measuring as applied to cell detection do not perform well in regions characterized by non-homogeneous physical parameters due, for example, to the presence of air–liquid interfaces or when the particle–electrode distance is relatively high. This paper presents a robust impedance measurement technique and a circuit for detecting cells flowing in microstructures such as microchannels and microwells. Our solution makes use of an innovative three-electrode measurement scheme with asymmetric polarization in order to increase cell detection ability in microstructures featuring large electrode distances of up to 100 μm as well as to limit signal loss due to cell position relative to the electrodes. Compared to standard techniques, numerical simulations show that, with the proposed approach, the cell detection sensitivity is increased by more than 40%. In addition, we propose a custom circuit based on division instead of difference between signals, as in standard differential circuits, so as to reduce the baseline signal drift induced by non-homogeneous conductivity. A simplified analytical model shows an increase in the signal-to-noise-ratio comprised in the range 3.9–5.9. Experimental results, carried out using an open-microwell device made with flexible printed circuit board technology, are in agreement with simulations, suggesting a six-fold increase of the signal-to-noise ratio compared to the differential measurement technique. We were thus able to successfully monitor the process of isolating K562 leukemia cells inside open-microwells determining all single-cell events with no false positive detection.

Introduction

The ability to detect and count cells and to pattern and analyze them is fundamental in many life-science areas ranging from cancer treatment to immunology and rare-cell study with applications in both diagnostic and therapeutic areas.[1–3]

Patterning of cells inside microstructures allows dynamic monitoring of cell characteristics and response to different kinds of stimuli such as the ones produced by interactions with other cells or molecules.[4–5] This kind of analysis is not feasible with standard flow cytometry techniques. Lab-on-a-chip and microfluidic devices have proved to be effective in providing integrated solutions to patterning and analyzing cells using various physical principles.[6] However, when it comes to sort out cells with specific properties, most of the microstructures proposed are not appropriate because they feature closed environments. Moreover FACS do not easily support cell sorting combined to dynamic analysis of cell functions. Conversely, open microstructures, *e.g.* open microwells,[7] have the advantage of enabling dynamic analysis of cell–cell interactions and cell recovery.

Monitoring of cells in open microstructures with label-free techniques not affecting cell functions is a novel issue still not addressed by other research works. Label-free detection overcomes the limitations imposed by standard flow cytometry techniques which, making use of optical detection, provide high-speed analysis but need optical labeling procedures (*e.g.* cell staining with fluorescent dyes) which are often labor-intensive and may interfere with cell functions and alter their response to stimuli.[8–12]

Electrical measurements to detect the temporal changes in impedance associated with the passage of cells have been used to perform impedance spectroscopy analysis.[13–14] Compared to optical ones, techniques based on electrical measurements are usually slower in terms of the number of detections obtainable per minute but do not need pre-treatment of samples and, thanks to microtechnology and fabrication capabilities, are more suited to highly parallel monitoring of different sites.[15–16] Following the Coulter counter approach,[17] several solutions have been proposed to achieve impedance monitoring by lab-on-a-chip technology and microdevices making use of differential schemes able to detect the mismatch between measurement and reference impedances.[8,9,13,15] To increase the detection sensitivity, the volume monitored should be noise-free and sized in order to reduce the cell–electrodes distance. However these two requirements cannot

[a]*ARCES – University of Bologna, Viale Pepoli 3/2, I-40123 Bologna, Italy. E-mail: afaenza@arces.unibo.it*
[b]*MindSeeds Laboratories, Via Fondazza 53, I-40125 Bologna, Italy*
† Electronic supplementary information (ESI) available. See DOI: 10.1039/c2lc40158d

always be guaranteed, especially when detection is not performed in standard microchannels.

On the one hand, in fact, the monitored volume may be much bigger than a single cell because it is deliberately sized to contain cell aggregates and allow cell–cell interactions or because of the limitations on electrode size and distance posed by microfabrication. On the other hand, the monitored volume may be characterized by the presence of physical non-homogeneity such as conductivity gradients, which may variously affect the measured and the reference impedances and offset the advantages of a differential approach. For example, the presence of heat sources or active electrodes placed near reading ones, may produce a local Joule-heating-induced impedance variation that influences differential measurements and lowers the signal-to-noise ratio. Another troublesome situation happens when performing impedance measurements in devices equipped with open interfaces whose use has been demonstrated to be effective in enabling simplified cell loading[7] and/or cell recovery procedures.[18]

In recent years devices based on open-interfaces have been proposed and have gained attention because of the advantages offered, for example, by pumpless capillary infusion of fluid inside microdevices,[19–20] or by evaporating-receding meniscus and surface tension.[21–24] Bocchi *et al.*[18] have proposed a device exploiting the capillary effect and surface tension based on open-microwells where cells can be delivered, processed, analyzed and then individually recovered thanks to the open outlet at the microwell air–fluid interface (Fig. 1). Microwell diameter is approximately 100 μm which allows for isolating both single cells and cell aggregates but, on the other hand, is several times larger than the typical dimension of microchannels devoted to electrical-based cell detection.

Impedance monitoring of cells in microstructures with a diameter in this order of magnitude and featuring open interfaces has not yet been addressed in existing works and practical solutions are still lacking.

Here we present a robust impedance measurement technique and a circuit to improve cell detection in large-volume regions with non-homogeneous physical parameters. Our approach uses both innovative asymmetric electrode polarization and a custom division-based circuit designed to increase the signal-to-noise ratio (SNR). We applied this novel technique to the detection of cells inside microstructures featuring open interfaces.[18] However, it could be used also in a variety of other different cases involving open-interfaces and large volumes such as: the procedure of cell spotting by using a droplet dispenser,[7,25] cell delivery in microwells by evaporating receding meniscus[21] or even when dealing with the simple procedure of cell dispensing inside a pre-filled microtiter array making use of a manual micropipette.

Fig. 1 shows a microstructure that has an open fluidic interface on the right and contiguous measuring electrodes. This simple model may be used throughout this work to make general comparisons between our measuring approach and existing ones.

The paper is organized as follows. After discussing the effects of both electrode polarization and localized noise sources, we analyze and compare the existing and the proposed measurement technique. The advantages produced by the latter in terms of reduced noise effect and increased sensitivity are numerically demonstrated. Finally, we report on experimental validation of impedance monitoring of single K562 leukemia cells delivered through microchannels in open microwells and compare analytical results with experimental ones.

Sensing technique and theory

Asymmetric electrode polarization

The standard measurement technique is based on three electrodes with symmetric polarization (Fig. 2a). The total current density is higher towards the sidewalls and therefore detection capacity, relying as it does on interference between a flowing cell and the current distribution in the microstructure, is lower at the center of the channel – which is the worst-case condition the electrical circuit must reckon with. Spencer *et al.*[26] demonstrated the detection of 6 μm polystyrene beads in a 40 μm microchannel independent from electrode–particle position. However, they showed that the best-case signal can be three times higher than the worst one that is improved using a relatively high stimulation amplitude (4 V in the cited article) which is not always recommended in order to reduce electrochemical processes as

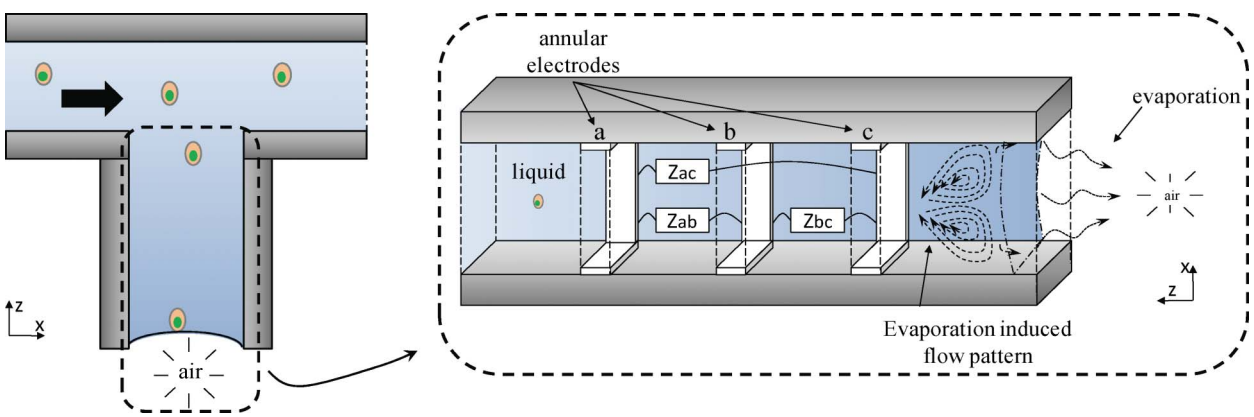

Fig. 1 (left) Cell isolation *via* microchannels.[18] Cells fall inside each microwell by gravitational force while capillary and surface tension prevents liquid from pouring out and the air–liquid interface acts as a virtual floor where cells can sediment. (right) 3D representation of the basic structure analyzed in this work consisting of a portion of microstructure (microchannel or microwell) featuring an open interface and a series of three electrodes. Three different impedance values (Z_{ab}, Z_{bc}, Z_{ac}) can be measured by choosing proper polarization schemes and sensing circuits.

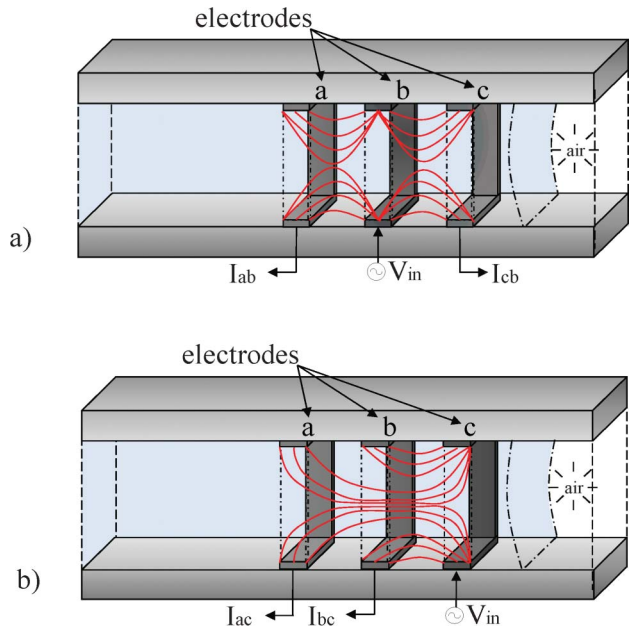

Fig. 2 (a) Standard 3-electrode symmetric polarization. (b) Asymmetric polarization scheme: excitation is applied to electrode c placed nearer to the air–liquid interface.

well as nonlinearities and avoid cell damage and a dielectrophoretic effect.[27]

One possible solution to overcome the detection capacity loss shown by the standard measurement scheme would be to apply the excitation to electrode c while using a and b for measurement. In this way, we obtain an asymmetric polarization (Fig. 2b) where some electric current streamlines are expected to be distributed close to the central part of the structure.

Choosing a frequency range allowing us to treat impedances as resistances, we may write:

$$\begin{cases} R_{bc} = R_0 \\ R_{ac} = kR_0 \end{cases} \quad (1)$$

where the value of k ($k > 1$) can be obtained through FEM simulations (see Results and discussion section).

The passing of a cell through a monitored volume is assumed to produce a variation ΔR_C whose value, as previously mentioned, depends on the interference between a flowing cell and current streamlines. Unlike the standard symmetric scheme where, for a given distance from the electrodes, the passing of a cell is detected in the same way by both impedances (R_{ab}, R_{bc}), when using asymmetrical polarization, the current streamlines connecting electrodes c and b are concentrated on the sidewalls and mainly detect cells flowing near the boundaries of the microchannel whereas the ones connecting electrodes c and a are forced to pass at the center and mainly detect cells aligned with the central horizontal axis of the volume monitored (see Results and discussion section). As a consequence, asymmetric polarization is expected to offer a better coverage of the monitored volume and helps to cut down the presence of blind-zones, thus making cell detection more stable and effective. In the next sections, standard differential and division measurement techniques, both coupled with asymmetric polarization, will be compared and analyzed.

Differential-based impedance measurement technique

The differential approach has been widely used to track impedance changes and detect cells in microstructures.[15] However using it with asymmetric polarization raises some problems when localized noise sources are considered.

If a noise source is located in proximity with electrode c, it will affect R_{bc} more than R_{ab}. This is what happens, for example, if a temperature variation or conductivity change due to evaporation occurs close to electrode c while temperature and conductivity at electrode a are kept constant due to their proximity to a liquid reservoir acting as a bulk (Fig. 3).

For our calculations we assume, in a simplified model, that the noise is maximum at electrode c and the induced local conductivity variation linearly decreases towards electrode a where it is zero (Fig. 3). Under this hypothesis the impedances will assume the form:

$$\begin{cases} R_{bc} = R_0 + 3\Delta R \\ R_{ac} = kR_0 + 4\Delta R \end{cases} \quad (2)$$

Assuming a signal frequency value where the impedance can be considered as a resistance, the differential amplifier (Fig. S1a in ESI†) combined with asymmetrical polarization subtracts the two voltages $V_1 = R_f I_{ac} = R_f V_{in}/R_{ac}$ and $V_O = R_f I_{bc} = R_f V_{in}/R_{bc}$ and the output voltage can be written as:

$$V_{out} = V_{in} R_f \frac{(R_{ac} - R_{bc})}{R_{ac} R_{bc}} \quad (3)$$

Both signal and noise variations are generally expressed by:

$$\Delta V_{out} = V_{out} - V_{out0} \quad (4)$$

where $V_{out0} = (V_{in} R_f (k-1)/(kR_0))$ is the output signal when $\Delta R_C = \Delta R = 0$ (no cell, no noise). Considering eqn (2) and the passing of a cell along the central horizontal axis of the structure, we

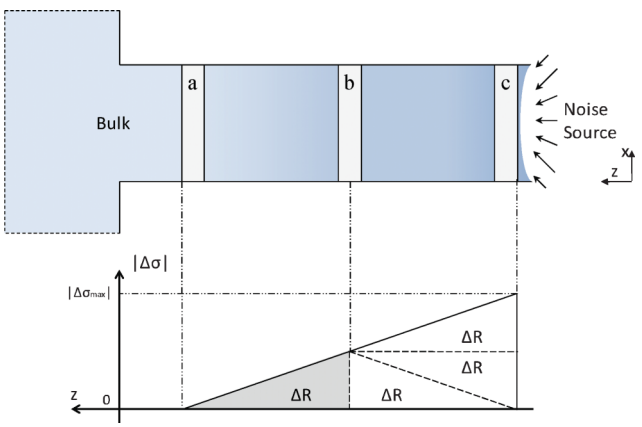

Fig. 3 A noise source localized in proximity with electrode c affects R_{bc} more than R_{ab}. This is what happens, for example, if a temperature variation or evaporation occurs at electrode c while the temperature at electrode a is kept constant due to proximity with a liquid reservoir acting as bulk. In our model we assume that the conductivity variation $\Delta\sigma$ is maximum at electrode c and linearly decreasing towards electrode a where it is zero. Integrating $\Delta\sigma$ in the two subvolumes a–c and b–c results in resistance variations $4\Delta R$ and $3\Delta R$ respectively.

obtain:

$$\begin{cases} R_{bc} = R_0 + 3\Delta R \\ R_{ac} = kR_0 + 4\Delta R + \Delta R_C \end{cases} \quad (5)$$

and the signal-to-noise ratio, under the approximation of small impedance change due to both cells and noise with respect to R_0, can be approximated as (see ESI†):

$$SNR_{diff,asym} = \frac{|\Delta V_{out}|_{noise=0}}{|\Delta V_{out}|_{signal=0}} \approx \frac{|\Delta R_C|}{|\Delta R(3k^2-4)|} \quad (6)$$

Division-based impedance measurement technique

The novel division-based solution performs impedance monitoring using three electrodes with asymmetric polarization and dividing the first output signal by the second one. The block diagram of the circuit is reported in Fig. S1b (see ESI†). The excitation signal is applied to electrode c placed nearer to the interface while two independent measurement branches measure the two impedances following the typical scheme of a lock-in amplifier. An *I*/*V* (current/voltage) conversion stage similar to the one in the differential circuit is followed by a preamplifier, an analog mixer which multiplies the amplified signal by the excitation one and a low-pass filter which isolates the DC value of the modulated signal.

The two output signals coming from the filters are then connected to the inputs of an analog divider. Since the impedance is approximated by a resistance, these two in-phase branches are sufficient for detecting resistance changes. If the goal of the system were to measure the exact value of amplitude and phase, then the proposed circuit would need to be duplicated by including the quadrature paths.

Under the same conditions as before, the output voltage of the analog divider V_{out} can be expressed as:

$$V_{out} = A_{div}\frac{R_{bc}}{R_{ac}} \quad (7)$$

where A_{div} is a conversion factor introduced by the divider circuit to convert the resistance ratio to voltages. As before, we can define the constant value $V_{out0} = A_{div}/k$, thus obtaining:

$$\Delta V_{out} = V_{out} - V_{out0} \quad (8)$$

which lets us express the SNR as (see ESI†):

$$SNR_{div,asym} = \frac{|\Delta V_{out}|_{noise=0}}{|\Delta V_{out}|_{signal=0}} \approx \frac{|\Delta R_C|}{|\Delta R(3k-4)|} \quad (9)$$

Materials and methods

Chip fabrication

We experimentally performed impedance monitoring on cells in a device composed of a 6 × 6 open-microwell array as depicted in Fig. 4. It was fabricated on a 3-layer flexible-PCB polyimide (DuPont, Wilmington, DE) substrate with copper metal layers and a total height of approximately 200 μm (device dimensions: 41.75 mm × 41.75 mm). The contour of the device is provided with pads for the electrical interface.

Each microwell is obtained by drilling 100 μm diameter through-holes in the metal layers. Three annular sensing electrodes called Top, Middle and Bottom (respectively a, b and c electrodes in the theoretical model) are thus created at each microwell and, in order to guarantee biocompatibility, are metalized with pure gold without creating any short-circuits between the different layers. Microchannels were created by soft lithography[28] on a photoresist film laminated onto a glass substrate. The microchannel structure was bonded to flexible PCB obtaining channels with a height of 55 μm, a width of 500 μm and a length of 4 cm. Microchannels are bonded on one side of the device so that microwells are found on the floor of them whereas the other side of the microwells is exposed to the air. For each microfluidic channel, two small pieces of a silicone tube were mounted as inlet/outlet ports (Fig. 4c).

Cell preparation and setup

K562 erythroleukemia cells (8–12 μm in diameter) were washed and suspended in PBS (composition: 137 mM NaCl, 2.7 mM KCl, 10 mM phosphate at pH 7.4, electrical conductivity 1.6 S m^{-1} @300 K, relative permittivity 80) at a concentration of 5 × 10^5 cells mL^{-1}. The cell suspension was loaded into a syringe infusion pump (KD210, KD Scientific Inc, MA, USA) and kept at a room temperature of 300 K and relative humidity of 40% throughout the experiment.

The infusion pump was connected to the inlet ports of the microchannels using 300 μm PTFE tubing (Watson-Marlow, MA) as shown in Fig. 4a. A custom measuring board controlled by a Labview program was connected to the chip placed on the stage of the microscope (Nikon Eclipse 80i, Tokyo, Japan). When a fluid is inserted in a microchannel, the microwells fill by capillarity and surface tension holds the liquid inside them, preventing leakage. If the fluid contains cells, these will flow inside the microchannel along the liquid and randomly fall inside the microwell (Fig. 4b and 4d). As a result, the meniscus at the air–liquid interface acts as a virtual floor for each microwell where cells can sediment, allowing for easier recovery procedures.[18]

Results and discussion

Effect of electrode polarization

Fig. 5a and Fig. 5b show the total current density norm in the top-half section of the 100 μm cylindrical microchannel of Fig. 4 using an 8-level contour map for both symmetric and asymmetric electrode polarization. In addition, current streamlines are used to disclose the current paths inside the monitored volume and allow determination of which couple of electrodes is responsible for the current density shown by the colour map. Looking at Fig. 5a, both streamlines and current density norm are equally and symmetrically distributed. A cell flowing from left to right aligned with the central axis produces over R_{ab} and R_{bc} equal and chronologically consecutive peaks which, when subtracted, lead to the double-peak graph usually reported in the literature. In the case of Fig. 5b, current density norm is higher in the region between electrodes b and c. The detection peak registered by R_{ac} and R_{bc} will therefore happen when the cell reaches the

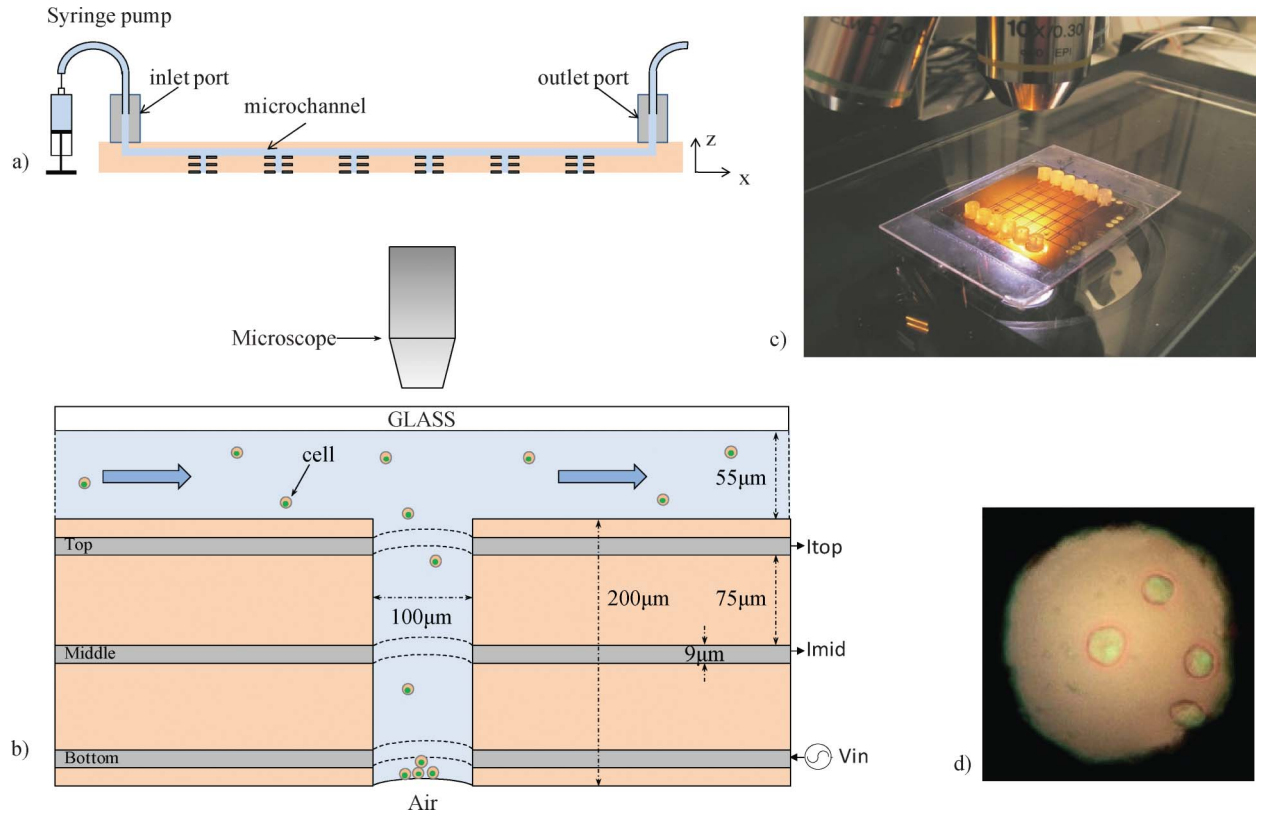

Fig. 4 (a) Device cross-section and (b) detail at an open microwell showing the process of cell isolation. (c) Photograph of device. (d) Microwell photograph taken with an upright microscope showing cells lying on the meniscus at the air–liquid interface.

highest current density region producing almost concurrent peaks whose amplitudes are, however, not equal as in the symmetric polarization case because of the not symmetric distribution of the current streamlines. As a consequence, the output signal obtainable with asymmetric polarization, either using a differential or a division based approach, does not resemble the typical double-peak signal (see "Cell detection" subsection).

It is possible to compute by FEM simulation the effective impedance variation due to a cell passing inside the volume monitored and quantify the improvement introduced by asymmetric polarization. Fig. 5c reports the maximum relative impedance variation due to a 10 µm cell passing as a function of the distance from the central horizontal axis, for both symmetric and asymmetric polarization (noise is not considered). On analyzing the two curves, one notes that the impedance variation increases as the distance from the border is reduced because the current density is higher on the sidewalls. On the central axis (distance equal to 0), which is the region where impedance variations are minimal, asymmetric polarization enhances them from 0.63% to 0.89% (41.2% increase). Hence, the overall detection sensitivity is increased by the same factor.

Determination of the form factor

The values of the resistances and capacitances for the electrical model representing an open microwell with the same geometrical parameters as found in Fig. 5, filled with phosphate buffer saline (PBS) and applying an excitation frequency of 100 kHz were obtained through FEM simulations (Comsol 3.5a) and are listed in Table 1 where we have separated the stray capacitances (subscript S) from those of the detection volume. At this frequency, the effect of the capacitances can be ignored, the error being inferior to 1%. R_{ac} is approximately three times higher than R_{bc} so in eqn (6) and (9) $k = 3$.

Effect of the measurement circuit scheme on noise drift compensation

For aqueous solutions, a one degree temperature variation produces a 2% conductivity change[29–30] which is comparable to the typical impedance change produced by a cell flowing through a microstructure.[13] Moreover, the speed of cells flowing inside a device may be very low if cell isolation is being carried out by means of cell free fall inside a microwell ($\approx$ 10 µm diameter cells have a sedimentation velocity of a few micrometres per second) so that temperature variations may have the same time constant as the signal and cannot easily be filtered or compensated by standard techniques.

Given the asymmetrical polarization, to compare the differential and the division approaches, one may calculate the ratio of the two SNRs of eqn (6) and (9) and determine the advantage given by the proposed approach (see ESI†). For a $\Delta R/R_0$ range [−10%; +10%], the SNR is increased by a factor between 3.9 and 5.9. Under the approximation of small impedance change due to both cells and noise with respect to R_0, can be expressed as:

$$\mathrm{SNRR} = \frac{\mathrm{SNR_{div}}}{\mathrm{SNR_{diff}}} = \frac{|3k^2-4|}{|3k-4|} \qquad (10)$$

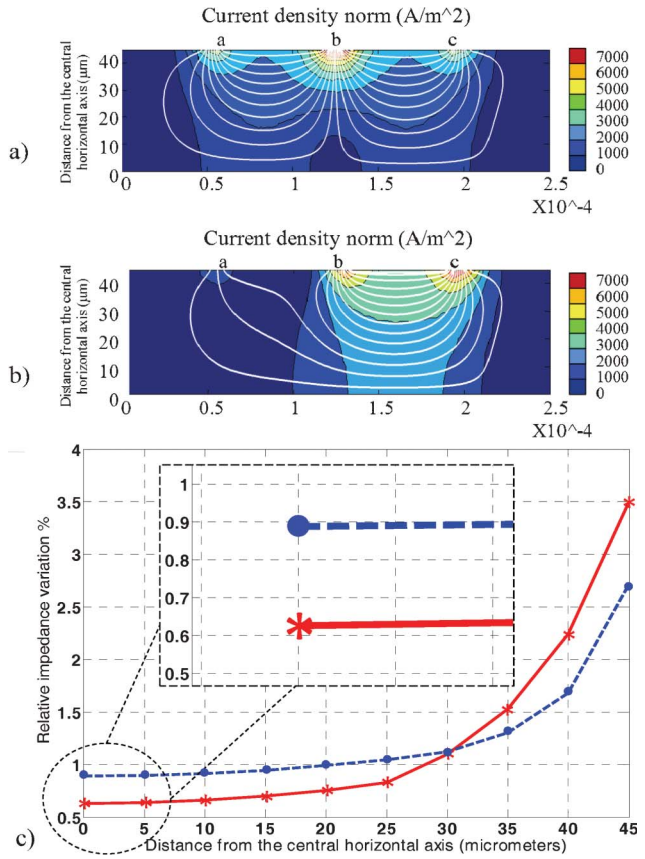

Fig. 5 (a) Symmetric polarization: simulation results of the total current density norm in the top-half section of the 100 μm cylindrical microchannel of Fig. 4 using an 8-level contour map. Current streamlines, depicted in white, are used to disclose the current paths inside the monitored volume and allow determination of which couple of electrodes is responsible for the current density shown by the colour map. The *x*-axis is the microchannel length while the *y*-axis represents the distance in micrometres from the central horizontal axis from 0 to 45 μm (microwell radius minus 5 μm cell radius). The voltage amplitude is 0.25 V at a frequency of 100 kHz. (b) Asymmetric polarization: simulation results of the total current density norm. Compared to (a), asymmetric polarization has a higher current density and, therefore, a higher detection ability for cell flow aligned along the central axis of the microchannel. (c) Comparison of performance between symmetric (solid line) and asymmetric (dashed line) polarization. On the *x*-axis the distance from the central axis of the monitored volume is plotted, on the *y*-axis the maximum relative impedance variation due to a 10 μm cell passing through. Noise is not considered. Geometrical and electrical parameters are the same as in (a) and (b).

Fig. S2, reported in ESI,† takes SNRR as expressed by eqn (10) varying k. Using the approximated eqn (10), the SNRR depends only on k and, for $k = 3$, is equal to 4.6 proving the efficiency of the proposed solution.

Table 1 Simulated resistance and capacitance values

$R_{top-bottom} = R_{a-c}$	46.9 kΩ @25 °C
$R_{middle-bottom} = R_{b-c}$	16.2 kΩ @25 °C
$C_{top-bottom}$	8.76 fF
$C_{middle-bottom}$	26 fF
$C_{s\ top-bottom}$	2 pF
$C_{s\ middle-bottom}$	3 pF

To compare the output drift induced by noise, we again used eqn (4) and (8) and calculated the ratio of the noise sensitivities in the two measurement techniques finding that, for $k = 3$, $\Delta R_C = 0$ and $\Delta R/R_0$ in the range [−10%; +10%], the proposed approach exhibits a variation which is from 4.8 to 7.2 times lower (see ESI†).

Comparison between model and experimental results

We tested our measurement approach by performing two tests: the first one to assess cell detection ability and the second one to demonstrate temperature variation auto-compensation without cells (a sort of noise-to-noise comparison).

Cell detection. To demonstrate the cell detection ability, we injected a buffer containing K562 cells at a concentration of 5×10^5 cells mL^{-1} into the microchannel (Fig. 4) and maintained a continuous 0.5 μL min^{-1} flow in order to deliver them to the microwells. The average number of cells trapped per well was 10 for an infusion time of 5 min. Fig. 6a shows detection of a cell inside an open microwell using the differential approach: the signal is severely affected by baseline drifting (approximately 1.65% ± 0.5% in 20 s) and software compensation is required for

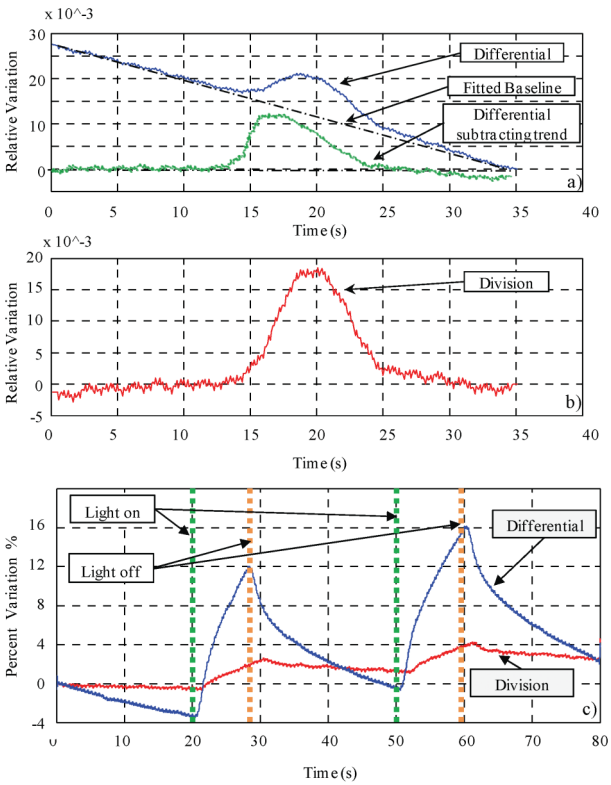

Fig. 6 (a) Detection signal of a K562 cell inside an open microwell using the standard differential approach and (b) the impedance division technique. (c) Comparison between differential and division measurement techniques, both with asymmetric polarization, in response to a temperature change induced by switching a 100 W microscope lamp on and off. Before switching of the light (0–20 s), the differential circuit shows a baseline drift which is not present in the division-based circuit output signal. After switching on, the division circuit undergoes a temperature-induced variation that is 5.35 times smaller than the differential circuit, proving the efficiency of the solution proposed.

peak detection and sizing. By subtracting the trend given by the fitted baseline using a software post-process algorithm, we detected single cells producing an output peak variation of 0.75% ± 0.44% (statistics based on 52 events).

Using the approach we propose, we found a similar output peak variation of 0.84% ± 0.57% but with a drift almost canceled (0.3% ± 0.2% in 20 s). Fig. 6b shows the detection signal given by the division circuit for the same cell as in Fig. 6a. As expected, the signals in the two approaches are comparable and, considering the natural non-homogeneity of cell size, are in line with the simulated values shown in Fig. 5c which, for asymmetric polarization, predicted a variation between 0.9% and 2.5% depending on the cell position. The average noise (drift) is, by contrast, 5.5 times lower using the division approach, a value similar to the one anticipated by eqn (10) with $k = 3$.

Setting a 0.1% threshold on the amplitude and a threshold on peak duration (between 5 and 15 s), we successfully detected all single-cell events, as confirmed by optical inspection with no false positive detection (0 false positive out of 52 detections). It was rare to find clusters of more than one cell flowing through (5 cases out of 52), though this situation was distinguishable as we typically measured an almost double pulse duration (Fig. S3 in ESI†).

Drift compensation. To demonstrate the efficiency of our scheme in reducing the temperature-induced drift, we heated the microwell in a worst case condition by alternately switching on and off a 100 W microscope lamp. This represents an asymmetric source of noise, as the lamp is positioned on the side of the open interface. An infrared thermometer was used to measure the actual temperature rise on the device surface, and found an increase by approximately 10 K in 10 s (from 300 K to 310 K) with almost linear overheating by 1 K per second. This translates into a resistance variation of about −20% in 10 s which, using the model depicted in Fig. 3, means a $\Delta R/R_0 = -5\%$, a −20% variation for R_{ac} and a −15% variation for R_{bc}.

The standard differential circuit together with asymmetric polarization with V_{in} = 1 V, R_f 20 kΩ, showed the behavior depicted in Fig. 6c: an initial downward drift from 0 to 20 s which is reversed when the heating lamp is switched on, increasing the monitoring signal by approximately 15% after 10 s. By way of comparison, the analytical model (see eqn (4) and ESI†) predicted an 18.7% variation for a 20% conductivity change and the values in Table 1. From $t = 0$ s to $t = 20$ s, the division circuit shows an output signal which is almost unaffected by drift. Comparing the relative signal variation from instant $t = 20$ s to $t = 30$ s in both of the approaches, the division-based one (2.8% variation) reduced the effect of the temperature-induced output variation by 5.35 times, a value similar to the 6.3 predicted by the analytical model for $\Delta R/R_0 = -5\%$ (see ESI†).

Signal-to-noise ratio. We compared the experimental SNRR to the one predicted by the model. Taking an average signal of 0.84% and 0.75% for the division and differential circuit and considering the noise reduction of 5.35 given in the previous section, the experimental SNRR is 6. The predicted value was 5.1. The difference between the two numbers can be attributed to the approximations introduced in the model such as the linear conductivity gradient (Fig. 3).

Conclusions

In this paper we have presented an impedance measurement technique to detect cells flowing through microdevices characterized by non-cell-sized geometrical dimensions and non-homogeneous temperature distribution such as labs-on-a-chip provided with open fluidic interfaces. Unlike standard measuring solutions based on 3 electrodes with symmetric polarization combined with a differential circuit, our solution makes use of innovative asymmetric electrode polarization together with a custom division circuit. Numerical simulations showed that, compared to existing solutions, the worst case detection signal is increased by more than 40%, the effect being to lower the typical sensitivity loss in the region furthest away from the electrodes. Moreover, the effect of noise due to evaporation and temperature variations with consequent non-homogeneous conductivity distribution is reduced by a factor in the range [4.8; 7.2], producing an increase in the signal-to-noise ratio in the range [3.9; 5.9]. Experimentally we delivered K562 cells inside an open-microwell based device and monitored the isolation process finding a correspondence between data and simulations for both noise reduction – which was 5.35 times (6.3 times expected) higher than the differential solution – and the cell detection signal which, setting a threshold on the peak amplitude and duration, allowed us to determine all single-cell events with no false positive detection with a SNR of 6 (5.1 expected).

References

1 M. Bocchi, *IEEE Trans. Electron Devices*, 2010, **57**(1), 244–255.
2 W. He, *et al.*, *Proc. Natl. Acad. Sci. U. S. A.*, 2007, **104**, 11760–11765.
3 A. Chung, *et al.*, *Cytometry, Part A*, 2006, **69A**, 142–146.
4 A. M. Skelley, *et al.*, *Nat. Methods*, 2009, **6**(2), 147–152.
5 J. C. Love, *et al.*, *Nat. Biotechnol.*, 2006, **24**(6), 703–707.
6 J. El-Ali, *et al.*, *Nature*, 2006, **442**(7101), 403–411.
7 M. Bocchi, *et al.*, *Biosens. Bioelectron.*, 2009, **24**(5), 1177–1183.
8 X. Cheng, *et al.*, *Lab Chip*, 2007, **7**, 746–55.
9 K. Cheung, *et al.*, *Cytometry, Part A*, 2005, **65A**(2), 124–132.
10 F. Vollmer, *et al.*, *Nat. Methods*, 2008, **5**(7), 591–596.
11 D. R. Gossett, *et al.*, *Anal. Bioanal. Chem.*, 2010, **397**, 3249–3267.
12 E. I. Galanzha, *et al.*, *Cytometry, Part A*, 2008, **73A**, 884–894.
13 S. Gawad, *et al.*, *Lab Chip*, 2001, **1**(1), 76–82.
14 J. Kruger, *et al.*, *J. Micromech. Microeng.*, 2002, **12**, 486–494.
15 S. Gawad, *et al.*, *Lab Chip*, 2004, **4**(3), 241–251.
16 S. B.Prakash, *et al.*, *IEEE Sens. J.*, 2007, **7**(3), 440–447.
17 W. H. Coulter, National Electronics Conference, Chicago, IL, 1956.
18 M. Bocchi, *et al.*, *Proceedings MicroTAS 2011*, 2011, 1722–1724.
19 V. Namasivayam, *et al.*, *J. Micromech. Microeng.*, 2003, **13**, 261–271.
20 M. Zimmermann, *et al.*, *Lab Chip*, 2007, **7**, 119–125.
21 M. C. Park, *et al.*, *Lab Chip*, 2006, **6**, 988–994.
22 S. Haeberle, *et al.*, *Lab Chip*, 2007, **7**, 1094–1110.
23 K. C. Hoang, *et al.*, *Anal. Chem.*, 2006, **78**, 1657–1664.
24 D. Juncker, *et al.*, *Anal. Chem.*, 2002, **74**, 6139–6144.
25 E. Duqi, *et al.*, *Sens. Actuators, A*, 2011, **168**, 320–327.
26 D. Spencer, *et al.*, *Lab Chip*, 2011, **11**, 1234–1239.
27 S. Gawad, *et al.*, *Rev. Sci. Instrum.*, 2007, **78**, 054301.
28 P. Vulto, *et al.*, *Lab Chip*, 2005, **5**, 158–162.
29 J. A. Sorensen, *et al.*, *Anal. Chem.*, 1987, **59**, 1594–1597.
30 P. M. Ramos, *et al.*, *IEEE Trans. Instrum. Meas.*, 2008, **57**(3), 577–583.